Collapse Mechanisms of Langmuir Monolayers

Ka Yee C. Lee

Department of Chemistry, Institute for Biophysical Dynamics, James Franck Institute, The University of Chicago, Chicago, Illinois 60637; email: kayeelee@uchicago.edu

Annu. Rev. Phys. Chem. 2008. 59:771–91

First published online as a Review in Advance on January 7, 2008

The *Annual Review of Physical Chemistry* is online at http://physchem.annualreviews.org

This article's doi: 10.1146/annurev.physchem.58.032806.104619

0066-426X/08/0505-0771$20.00

Key Words

lipid, folding, lung surfactant, interfacial elasticity, fluorescence

Abstract

When a two-dimensional (2D) film is compressed to its stability limit, it explores the third dimension via collapse. Understanding this 2D-to-3D transition is of great importance as it provides insight into the origin of defects in thin films. This review draws attention to a reversible folding collapse first discovered in model lung surfactant systems and explores the driving forces for this mechanism. The mode of collapse can be tuned by varying the mechanical properties of the film. I present a continuum elastic theory that captures the onset of the observed folding instability and use digital image analysis to analyze the folding dynamics. This article further explores factors that determine the maximum surface pressure a mixed monolayer can sustain and explains the observed phenomenon using the principle of rigidity percolation. The folding transition observed in lipid monolayers described here has also been observed in other systems, including monolayers of nanoparticles.

INTRODUCTION

Langmuir monolayers provide a unique way of studying two-dimensional (2D) materials at asymmetric interfaces, and investigations of Langmuir monolayers have uncovered a rich variety of physical phenomena (1–3). Whereas researchers have routinely employed monolayers of chemical surfactants at air-water or oil-water interfaces in a variety of applications—from reducing interfacial tension, to controlling wetting properties and stabilizing emulsions and foams (4, 5)—they have more frequently used monolayers of biological surfactants, such as phospholipids, to elucidate lipid-protein interactions and to mimic the surfaces of cell membranes (6–9). In most of these cases, the desired thin film is a contiguous, stable, 2D assembly of the surfactant molecules, in which the packing density of the molecules is not at its maximum. Earlier work has uncovered a great deal about the polymorphism and 2D phase transitions of these monolayers (2, 6, 7, 10). What is less understood, however, is how such a film, when compressed to the limit of its stability in two dimensions, explores the third dimension upon monolayer collapse. Understanding this 2D-to-3D transition is of great importance as it provides insight into the origin and nature of defects in thin films such as those that coat optical fibers (11, 12) and biological ones that protect the eyes (13, 14), the ears (15, 16), and the inner surface of our lungs (17–19).

Over the past few years, the evolution of Langmuir trough designs that can sustain high surface pressures, coupled with techniques such as laser light scattering (20, 21), fluorescence (22), and Brewster angle microscopy (23–25), has allowed us to visualize the morphology of monolayer collapsed structures (26–31). These observations let us get at the driving forces and mechanisms responsible for monolayer collapse. For the case of lung surfactant (LS), a mixture of lipids and proteins that coats the alveoli (32), monolayer collapse (which occurs at the end of exhalation) is of particular importance: Attaining a low surface tension at collapse is crucial for lessening the work of breathing, and the ability to reincorporate collapsed materials upon inhalation is essential for proper functioning of the lung. This review describes the peculiar ability of LS monolayers to undergo a novel reversible collapse. Learning from this specific system, we generalize our observations and delineate the physical parameters accountable for such a reversible collapse. We demonstrate how the mode of collapse can be tuned by varying the mechanical properties of the film and provide a theoretical framework for the observed collapse behavior. Finally, this review explores how the composition of a lipid mixture can affect the collapse pressure of the film and makes possible connections between the collapse observed in organic films of nanometer thickness to the collapse of other types of materials.

MONOLAYER COLLAPSE

At large areas per molecule, amphilphilic molecules in a monolayer are in the gaseous phase, with their hydrophobic portions making significant contact with the water surface but little contact with each other (33). Area reduction causes a series of 2D phase transformations (1–3, 7, 10). At a low surface density, the surfactant does little to alter the surface tension, γ, giving rise to a zero surface pressure, π (where π

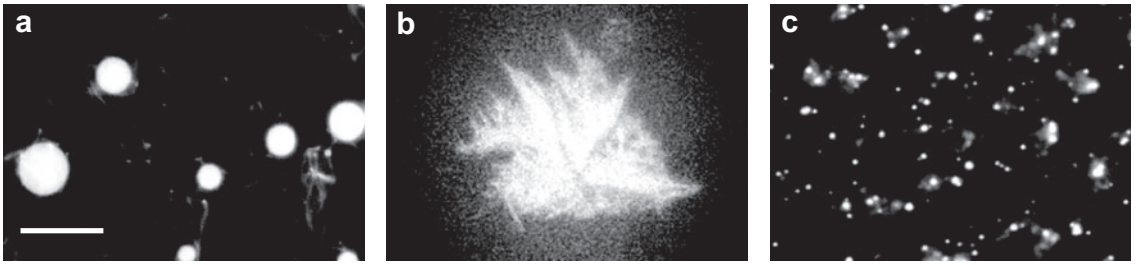

Figure 1

Fluorescence micrographs of monolayer collapse from single component films of different fluidity (*a*, *b*), and monolayer squeeze out in a binary mixture (*c*). (*a*) The collapse of the fluid film POPC on water at 25°C, at which both bilayer disks and tubes are formed during collapse. (*b*) The collapsed structure from a rigid palmitic acid film on water and at 16°C, at which dendritic growth of a crystalline phase is seen above the monolayer. (*c*) The squeeze out of the more fluid component, POPG, from a binary mixture of DPPG and POPG on water at 23°C. The squeeze out of POPG from the film at the plateau region in the isotherm leaves the film enriched in the more rigid component, DPPG. The scale bar is 50 μm. Figure adapted from References 38 and 72.

is the surface tension at a pure air-water interface, γ_0, minus the surface tension at the interface with monolayer adsorbed, γ). As the monolayer is compressed into the liquid-expanded (LE) phase, the hydrophobic parts of the molecules come into contact with each other, but remain largely disordered and fluid. As a contiguous LE film is formed, the isotherm lifts off, giving rise to a positive surface pressure. Further compression leads to a first-order transition to the condensed (C) phase, marked by a plateau in the isotherm corresponding to the LE and C coexistence. Compression of the C phase results in transitions to different ordered phases similar to those found in liquid crystals (34). Eventually, the molecular area (or π) reaches a limiting value beyond which the monolayer cannot be compressed further without destabilizing its 2D nature and yielding structures in the third dimension (35, 36). The surface pressure at collapse, π_c, determines the minimum surface tension for a monolayer, whereas the collapse mechanism determines its reversibility (i.e., how well the monolayer respreads upon expanding the film). In general, fluid monolayers such as those formed by lipids above their critical temperatures have relatively low π_c and collapse via the ejection of materials to the subphase (**Figure 1*a***) (37–39). More ordered and rigid monolayers collapse at higher π_c, usually by fracturing, followed by a loss of materials in the subphase or the formation of multilayered aggregates at the air side of the interface (**Figure 1*b***) (40–43). Via either mechanism (fracture or solubilization), collapse is irreversible, and the collapsed materials do not reincorporate into the monolayer as the surface pressure is decreased (38, 42, 44, 45).

MONOLAYER SQUEEZE OUT

When a binary mixture comprises lipids with different collapse pressures (e.g., unsaturated lipids with low π_c and saturated lipids with high π_c), the resulting isotherm usually exhibits a plateau at a pressure corresponding to the lower collapse pressure

of the more fluid component, with the ultimate collapse pressure similar to that of the more rigid component. Fluorescence and Brewster angle microscopy images of a binary mixture of dipalmitoylphosphatidylglycerol (DPPG; higher π_c) and palmitoyloleoylphosphatidylgycerol (POPG; lower π_c) show that POPG is indeed excluded or squeezed out from the monolayer over the plateau region, leaving the film enriched in the more rigid component at high surface pressures (**Figure 1*c***) (46, 47). The squeeze out of the more fluid component is in effect the solubilization process described above, which renders it irreversible.

ELIMINATION OF SQUEEZE OUT AND INDUCTION OF REVERSIBLE FOLDING IN LUNG SURFACTANT MONOLAYERS

Investigators have used the squeeze-out hypothesis to explain the isotherm of LS (44, 48–50) that also exhibits a plateau at high surface pressures below the ultimate π_c. As mentioned above, LS is a complex mixture of lipids and proteins that lines the alveoli and is responsible for proper functioning of the lung (51). LS works both by lowering the surface tension to reduce the work of breathing and by stabilizing the alveoli through varying the surface tension as a function of alveolar volume. To accomplish this, it must adsorb rapidly to the air-fluid interface of the alveoli after being secreted. Once at the interface, LS must form a monolayer that can both achieve low surface tensions upon compression and vary the surface tension as a function of the alveolar radius (44).

Saturated, zwitterionic dipalmitoylphosphatidylcholine (DPPC), which can form monolayers that reduce surface tensions to near-zero values (and thus is responsible for reducing the work of breathing), constitutes a major component of LS. However, DPPC adsorbs and respreads slowly as a monolayer under physiological conditions, making it by itself a far from ideal LS candidate. The unsaturated and anionic lipids and cationic proteins in natural LS are thought to enhance the adsorption and respreading of DPPC (52). However, owing to their relatively low collapse pressure, LS monolayers are thought to be refined by the selective removal of species with low collapse pressures on repeated compression and expansion, leaving behind a monolayer enriched in lipids that promote low surface tension (48, 53–57). If the squeeze-out hypothesis were correct, the composition of LS would be altered in each exhalation process, rendering it necessary to reconstitute the LS composition in each breathing cycle.

The squeeze-out hypothesis for LS, however, neglects the possible synergistic interactions among the various LS components that can alter the phase behavior of the mixed system. In fact, when cationic lung surfactant protein B (SP-B) is added to a binary mixture of anionic DPPG and POPG, squeeze out of POPG (**Figure 1*c***) is eliminated in the ternary mixture even though a plateau is still evident in the isotherm. The plateau in this ternary system is reproducible upon cyclic compression, suggesting that even if there were material loss, the material is somehow reincorporated into the film upon expansion, and the film behaves in a similar manner in subsequent cycles (46, 47). Fluorescence microscopy reveals a clear difference in the surface morphology

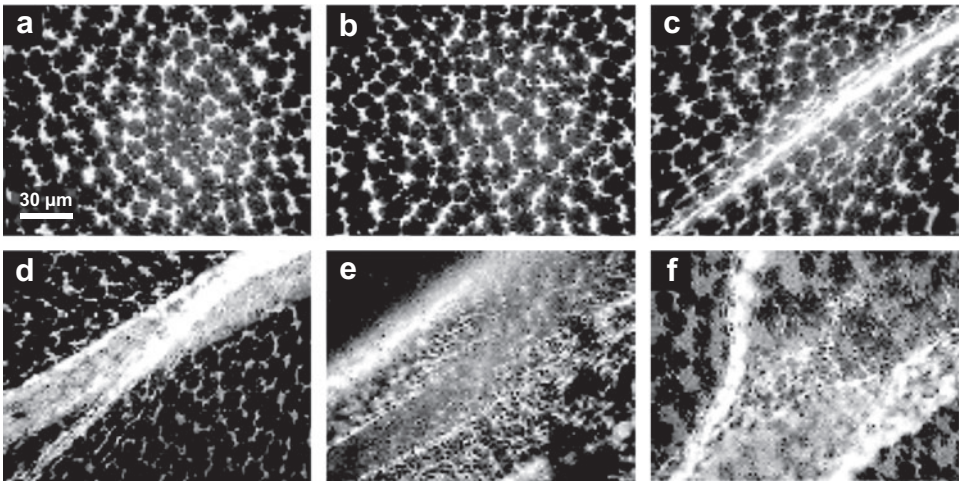

Figure 2

Fluorescence microscope images of a 3:1 mol:mol DPPG:POPG monolayer containing 10 wt% SP-B protein on a pure water subphase at 30°C, showing (*a*, *b*) the retention of the bright phase in the interstitial regions in the monolayer (*a*) through the high-pressure plateau region and (*b*) up to collapse, the (*c*) nucleation and (*d*) growth of a folded region, (*e*) the existence of the same domain morphology within the fold as within the overlying monolayer, and (*f*) the unzipping and reincorporation of the folded region upon expansion. Figure adapted from Reference 47.

at the plateau region between the binary and the ternary systems. In the absence of SP-B, squeeze out of POPG is observed. The departure of POPG-rich vesicles into the subphase renders the images blurry (**Figure 1*c***). With SP-B present, however, compression through the plateau region does not give rise to any vesicle detachment (46–47). Instead, the structure of the domains remains intact, with changes observed only in fluorescence intensity at the interstitial region (**Figure 2*a*,*b***). The increase in fluorescence intensity signifies an enhanced amount of fluorophores in the interstitial region—a point to which we return in the next section.

Intriguingly, the addition of SP-B not only eliminates squeeze out of the lipid component with a lower π_c, it also causes the film to collapse via a novel mechanism. Unlike the fracturing or the solubilization processes described above for rigid and fluid films, respectively, this ternary mixture buckles upon collapse, forming protrusions that extend several microns into the subphase (46, 47, 58). The buckled regions occur at random and coexist with the undeformed, flat monolayer (**Figure 2*c***). Further compression changes the fraction of the monolayer in the folds relative to the flat regions at a constant collapse pressure (**Figure 2*d***). These folds are different from the previously observed second-order buckling transition in which uniform, nanometer-amplitude undulations were observed experimentally (59, 60) or predicted theoretically (61, 62). The monolayer remains biphasic all the way up to collapse, with a network of the disordered bright phase surrounding islands of the ordered dark phase (**Figure 2**). Similar morphology is found within the fold, as well as on the

flat monolayer, suggesting that the film does not undergo any refinement process, in contrast with the squeeze-out hypothesis. The novelty of this folding collapse is its reversibility: Upon expansion of the film, the folded pleats open, starting from the edge of the collapsed structure (**Figure 2*e***), and the materials in the folds are reincorporated into the lipid film (**Figure 2*f***) (46, 47, 58). This drastic change in the collapse mechanism suggests a synergistic effect between the anionic lipids (with low π_c) and the cationic SP-B peptides that may result in the retention of both components upon collapse and their reincorporation into the monolayer upon expansion. A similar folding transition has also been observed in a model synthetic LS monolayer (63) comprising 67% DPPC, 22% POPG, 8% palmitic acid (PA), and 3% SP-B by weight (58).

To better understand why the interstitial region becomes brighter as one transverses the plateau region (**Figure 2*a***), researchers have obtained, using atomic force microscopy, higher-resolution images of these monolayers after their deposition from the air-water interface onto a mica substrate (46, 47, 64). The atomic-force micrograph in **Figure 3** indicates that instead of being lower in height than the C phase domains owing to the greater tilt of the acyl chain, the disordered interstitial region is higher by the thickness of a bilayer or multiple thereof (46, 47). In effect, the presence of the peptide makes possible the coexistence of a flat monolayer and multilayers. In the absence of the peptide, the anionic lipid component with the lower π_c would have been squeezed out at the plateau, leaving a film constituted mainly by the C domain region. The elimination of squeeze out likely results from the electrostatic interactions between the cationic SP-B and the anionic lipids, preventing the latter from being expelled from the interface. The reversibility of this folding collapse mechanism further makes it possible for the LS materials to be reused in subsequent breathing cycles, making this a much more plausible mechanism than that of squeeze out for the proper functioning of the lung. In fact, electron microscopy images of alveoli have revealed a coexistence of monolayer and multilayer LS structures lining the alveoli in animals (65). The folded collapse structures observed in these model systems likely provide 3D associated reservoirs that serve as temporary depositories for the excess materials at the end of the exhalation process.

FOLDING TRANSITION AS A GENERAL COLLAPSE PHENOMENON

Although the first instance of folding collapse was observed in LS monolayers, subsequent work has demonstrated that this type of collapse phenomenon can be observed in other systems under appropriate experimental conditions. Anionic DPPG and zwitterionic dipalmitoylphosphatidylethanoamine do not fold upon collapse at pH 5.5 in water, but both undergo folding in a 2-mM Ca^{2+}, 150-mM NaCl, 0.2-mM $NaHCO_3$, pH 6.9 subphase. Zwitterionic DPPC by itself has not been observed to fold under all subphase conditions tested, but when anionic PA or zwitterionic hexadecanol (HD) is added to the film beyond a certain threshold value, folding occurs at these mixed monolayers as well. Although a DPPG/POPG/SP-B monolayer folds on a pure water subphase, the addition of 150-mM NaCl eliminates any folding

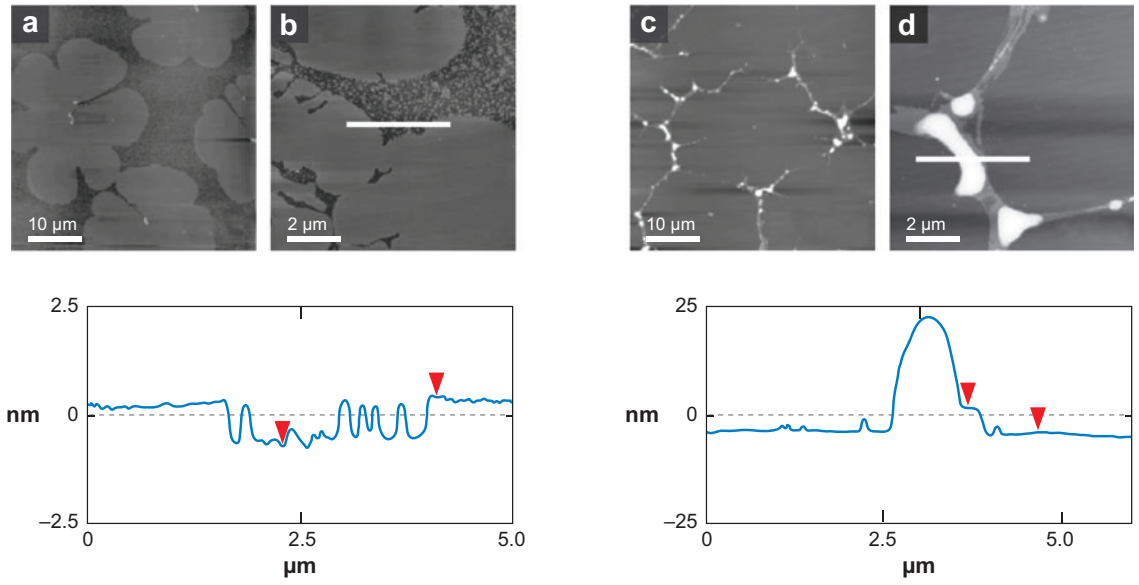

Figure 3

(*a*) 50 × 50 μm and (*b*) 10 × 10 μm contact-mode atomic force microscopy (AFM) images of 3:1 DPPG:POPG/10 wt% SP-B monolayers transferred to mica substrates at a surface pressure below the high-pressure plateau ($\pi = 40$ mN m^{-1}). (*a*) Before the plateau, the typical morphology is flower-shaped condensed (C) phase domains in a continuous liquid-expanded (LE) phase (compare to the fluorescence images in **Figure 2*a*)**. (*b*) Higher magnification of the LE phase, which contains many small ordered C domains. The white line on the image shows the location of the height trace shown below. The arrows on the height trace show the approximate height difference, which is 1.1 nm. The C domains are higher than the LE phase, and the small domains are the same height as the C domains. (*c*) 50 × 50 μm and (*d*) 10 × 10 μm contact-mode AFM images of 3:1 DPPG:POPG/10 wt% SP-B monolayers transferred to mica substrates at a surface pressure above the high-pressure plateau ($\pi = 55$ mN m^{-1}). (*c*) The domains of C phase have their flower-shaped structure somewhat distorted and are more compact; they are still separated by a continuous disordered phase, which is now of variable thickness. (*d*) Higher magnification of the disordered phase material. The white line on the image shows the region of the line trace. The arrows on the height trace show the approximate height difference, which is 5.2 nm, approximately the thickness of a bilayer of these lipids. The globule shown is approximately 30 nm high from the C domain to its top. The disordered phase domains appear to form multilayer patches rather than completely lose their material to the subphase. Figure adapted from Reference 47.

transition. Interestingly, further addition of 2-mM Ca^{2+} acts to reintroduce folding back into the system (66). All these observations suggest that the folding transition is a more general collapse phenomenon. In particular, the disappearance of folding upon the introduction of monovalent ions (which fluidizes the film) and the re-emergence of folding upon collapse with the addition of divalent ions (which rigidifies the film) suggest that the mechanical properties of the film may dictate the route for this 2D-to-3D transition. The notion is further supported by the observation of folding in DPPC monolayers when enough PA or HD is introduced (67). From the molecular

geometry viewpoint, the cross-sectional area of the tail is small compared with that of the head for DPPC, and even at high surface pressure, grazing angle X-ray diffraction data show that the acyl chains are still tilted (67–69). The opposite, however, holds true for both PA and HD, and the tails are in the most close-packed hexagonal configuration even at relatively low surface pressures (67, 70, 71). We can thus view PA or HD as wedge molecules, and their addition to the DPPC film helps prop up the acyl chains of DPPC, enabling the system to pack more tightly (67). Researchers have observed a somewhat different yet related type of folding transition resulting in the formation of convoluted giant folds in monolayers of 2-hydroxytetracosanoic acid (21, 31).

One can make a macroscopic analogy of the modes of collapse in these nanoscopic films. When a piece of stiff material such as glass is subjected to stress, the only way for it to relieve the stress is to fracture or crack. Conversely, objects such as balls floating in an air-water interface, when compressed to an area smaller than their total cross-sectional area, undergo rearrangements by desorbing to the subphase or superphase. We can draw parallels between these two macroscopic examples and the two types of 2D-to-3D transitions observed for rigid and fluid monolayers. The reversible folding transition, conversely, is similar to the manner by which a thin sheet of paper responds to a lateral stress—upon compression, the paper buckles and folds. Thus, it appears that in all Langmuir monolayer systems that undergo the folding transition, their mechanical properties fall within a certain Goldilock window of rigidity: The monolayer is neither too rigid nor too fluid, but just right for the observed folding to take place.

If the mechanical properties of the system did dictate the mechanism of collapse, then one could possibly alter the route by which a monolayer collapses by tuning its mechanical properties. This can be most simply achieved by varying the temperature: The system should be more rigid at a low temperature, and the same system should be more fluid at an elevated temperature. Concurrent study of the microscopic phase behavior, morphology, and surface pressure–area isotherms of Langmuir monolayers of a 7:3 mixture of DPPC and POPG at various temperatures between 20 and 40°C clearly demonstrates this point (29). At temperatures below 28°C, the DPPC:POPG monolayer is biphasic and collapses by forming large-scale folds, which reliably unfold upon expansion (similar to that shown in **Figure 2**). Above 33.5°C, the monolayer is homogeneous and, upon further compression, prefers to collapse through micron-scale vesicular structures that are globular or tubular in shape. **Figure 4** shows the equivalent of a pressure-temperature phase diagram for these 2D-3D transitions. In this quasi–phase diagram, the nucleation pressures of the folding transitions and vesicle formation are plotted against their corresponding temperatures, and the diagram indicates a first-order-like transition between the two collapse modes modulated by temperature. Collapse occurs via both folding and vesiculation at temperatures between 28 and 33.5°C, leading to the coexistence of the monolayer with both folds and vesicles (29). Analogous to equilibrium phase transitions, there may exist a temperature in this range that can be thought of as a triple-point temperature for the coexistence of the three phases corresponding to a 2D monolayer, 3D folds, and 3D vesicles.

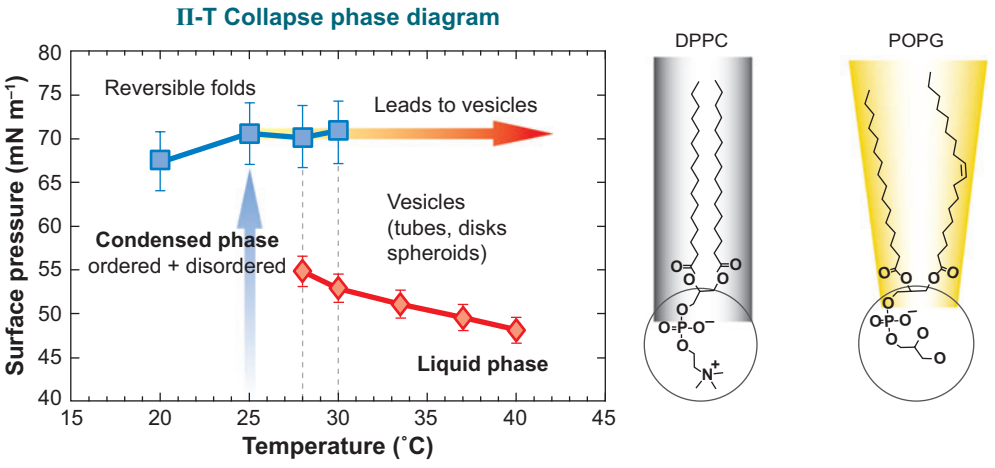

Figure 4

Surface pressure (Π) versus temperature (T) phase diagram for a 7 DPPC:3 POPG binary mixture. The blue squares indicate the point of nucleation of the folding transition, and the red diamonds indicate the point of abrupt increase in budding of vesicle-like structures. The vertical and horizontal arrows indicate the isothermal compression and isobaric heating of the monolayer, respectively, during the heating experiment. Figure adapted from Reference 29.

In addition to this triple point, the mode of collapse should be independent of the path taken in the temperature-pressure parameter plane. Indeed, one can obtain vesiculation either by compressing a fluid monolayer at 35.5°C or by first compressing a more rigid film at 25°C up to the folding transition, followed by heating the system to the final temperature of 35.5°C (**Figure 4**); **Figure 5** shows a corresponding series of monolayer morphological images captured during the heating process (29).

ELASTIC THEORY FOR THE ONSET OF FOLDING INSTABILITY

The Monolayer as an Elastic Sheet

As shown in **Figure 2**, both the lateral structure of the monolayer and its 3D structures upon collapse are of micron size, a length scale much larger than the molecular scale. One can use a continuum description of the monolayer as an elastic sheet at high surface pressures. There are various experimental indications that model LS monolayers may be at biphasic coexistence during a large portion of the compression-expansion cycle (29, 42, 47, 58, 72, 73). The theoretical model used for understanding the driving force for the folding transition observed experimentally therefore needs to consider a heterogeneous elastic sheet. As shown below, heterogeneity plays a major role in determining the 3D structure and stability of the film.

The two sides of the monolayer are not identical—on one side there are lipid head groups facing an aqueous phase, whereas on the other there are hydrocarbon tails facing air. This asymmetry implies a natural tendency of the monolayer to bend; in

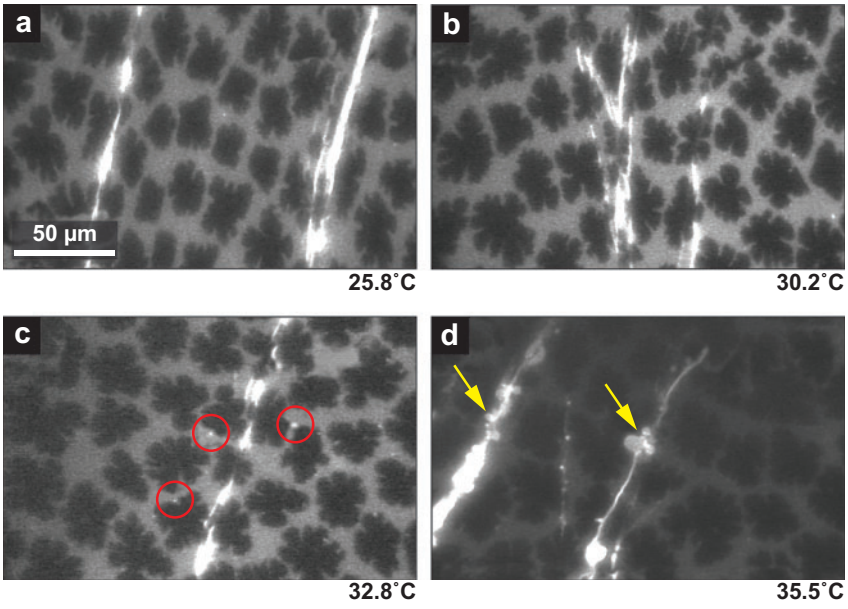

Figure 5

Fluorescence micrographs of a 7:3 DPPC:POPG monolayer at different temperatures during the heating experiment. (*a*) At 25.8°C, the predominant collapse structures observed are folds. The monolayer shows a few vesicles (*white spots*) along with folds, but they are not significant in number. (*b*) At 30.2°C, the monolayer does not show any considerable change from panel *a*. (*c*) At 32.8°C, the monolayer shows a large number of vesicles being formed at the boundaries between the condensed (*dark gray*) and disordered (*light gray*) phases, circled in red. This abrupt increase in the number of vesicles normally starts between 31 and 33°C. Beyond 33°C, the vesicles bound to the monolayer or the folded region either fuse to form larger ones or detach and diffuse into the subphase. (*d*) At 35.5°C, the region in focus shows the formation of vesicles from the folds below the plane of the monolayer. The yellow arrows indicate regions where smaller vesicles have fused to form larger ones. Figure adapted from Reference 29.

other words, the monolayer sustains a spontaneous curvature (5, 74). Apart from the molecular contribution, the spontaneous curvature can also have an electrostatic one (75). Both contributions typically amount to a radius of curvature of the order of a few nanometers. Opposing bending is the air-water interfacial tension, which progressively decreases upon monolayer compression from approximately 72 mN m^{-1} at low-lipid surface density to as low as only a few mN m^{-1} at high-lipid surface density prior to monolayer collapse. For example, DPPC can attain a surface tension close to 0 mN m^{-1} when it is compressed to its tightest possible packing.

A minimum model for the folding monolayer is that of a heterogeneous elastic sheet with bending rigidity K, surface tension γ, and a spontaneous curvature c_0 that has differing values (c_{01} and c_{02}) in the two domain types. The bending rigidity of a highly compressed lipid monolayer is typically a few hundred times the thermal energy k_BT, where k_B is the Boltzmann constant and T the absolute temperature (76). One can also consider differing values of K for the two types of domains involved, yet

the results remain qualitatively the same (77). As we only consider elastic deformations of such a sheet, whose energy is much larger than both $k_B T$ and the gravitational cost of the consequent contortion of the water surface (78), the model is static and purely elastic, neglecting thermal fluctuations and gravitational effects.

The elastic parameters K and γ define a new length, $\lambda = (K/\gamma)^{1/2}$, which determines the lateral extent of elastic deformations. Experimentally obtained values give a λ of the order of a few nanometers. Thus, both $(c_0)^{-1}$ and λ are of nanometer scale, much smaller than the domain size (tens of microns). For any biphasic structure far from a critical point, the typical width of domain boundaries is also not larger than a few molecules. This allows us to focus on a single domain boundary and assume that it is straight and sharp and separates two very large phases. Such a structure can be parameterized by its local angle $\theta(s)$ with respect to a reference plane at arc-length s from the boundary. The elastic energy of the monolayer (per unit length of boundary) is then a functional of the topography $\theta(s)$:

$$g[\theta(s)] = \int_{-\infty}^{\infty} \mathrm{d}s \left[\frac{1}{2} K \left(\frac{\mathrm{d}\theta}{\mathrm{d}s} \right)^2 - K c_0 \frac{\mathrm{d}\theta}{\mathrm{d}s} + \gamma(1 - \cos\theta) \right], \quad (1)$$

where the first two terms are the bending energy owing to deviations of the local mean curvature $c(s) = \mathrm{d}\theta/\mathrm{d}s$ from the spontaneous curvature c_0, and the last term is the tensile energy associated with deviation from a flat state.

Mesa Topographies

The static shape of the monolayer close to a domain boundary is the one that minimizes Equation 1. The somewhat surprising result is that, as long as the domains differ in their elastic parameters (i.e., $c_{01} \neq c_{02}$), the sheet is always inflected at the domain boundary. This implies that domains of different phases, owing to the different materials properties, have different heights. In other words, the biphasic structure is accompanied by a 3D topography of mesas. Far away on one side of the boundary, the monolayer is subjected to a torque $Kc_{01} - \gamma h_1$. Similarly, far away on the other side acts a different torque of $Kc_{02} + \gamma h_2$. For the monolayer to remain stationary, these torques must balance each other; hence,

$$h = h_1 + h_2 = \frac{K(\delta c_0)}{\gamma} = \lambda^2(\delta c_0), \quad (2)$$

where $\delta c_0 = c_{01} - c_{02}$. The height difference h increases with the contrast in spontaneous curvature δc_0, rigidity K, and compression (i.e., decrease in γ). For moderate compression, where γ is equal to a few tens mN m^{-1}, h is typically not larger than a few angstroms, yet at high compression ($\gamma \sim 1$ mN m^{-1}), it may reach a few nanometers. Because of these small values, and the fluidity of the interface, mesas have not been decisively observed, even though there have been hints of their possible existence (79, 80).

To obtain the topography in more detail, we should minimize Equation 1 with respect to $\theta(s)$ while requiring that the monolayer be flat far away from the domain boundary, $\theta(s \to \pm\infty) = 0$, and continuous at the boundary, $\theta(s = 0^-) =$

$\theta(s = 0^+) = \theta_0$. The resulting topography is given by (77, 78)

$$\tan\frac{\theta(s)}{4} = \tan\frac{\theta_0}{4}\exp\left(-\frac{|s|}{\lambda}\right), \qquad \sin\frac{\theta_0}{2} = \frac{\lambda(\delta c_0)}{4}. \tag{3}$$

Upon compression (decreasing γ and increasing λ), the inflection becomes sharper and higher, subsequently developing a stable overhang.

Instability

When $\lambda(\partial c_0) > 4$, i.e.,

$$\gamma < \gamma_c = \frac{1}{16}K(\delta c_0)^2, \tag{4}$$

the solution obtained for the monolayer topography becomes invalid. This marks an instability in which the monolayer's resistance to further compression vanishes. Note that this elastic instability occurs at positive surface tension. At instability, the monolayer in the vicinity of the boundary is expected to undergo a shape transformation to another state, which is determined by factors outside the simple elastic model presented here (e.g., the observed localized folds). In fact, we expect the new state to become energetically favorable before the instability condition (Equation 4) is reached, thus making the transition abrupt (first order) rather than continuous (second order).

One mechanism recently suggested as a driving force for fold formation is monolayer-monolayer adhesion into a bilayer (76). In homogeneous monolayers, the formation of a fold through adhesion requires overcoming nucleation barriers much higher than k_BT. Thus, the mesa topography in a biphasic monolayer and its elastic instability could provide a way to reduce and eliminate these barriers. This supports the conjecture that a biphasic structure of monolayers like that of LS is a necessary condition for its efficient folding upon compression (29, 73).

WHAT DETERMINES THE COLLAPSE PRESSURE?

The previous sections describe the various modes of collapse that a 2D monolayer can undergo, depending on its various materials (and hence mechanical) properties and use an elastic theory to interpret the collapsed structures observed. As a variety of applications use mixed lipid systems, a question that naturally arises is whether the maximum surface pressure sustained by a monolayer can be determined from its composition. In other words, for a simple two-component system in which the collapse pressures of the individual components are significantly different, how does the collapse pressure change when the relative amounts of the two are varied? To address this question, systematic studies on binary lipid mixtures with varied compositions need to be carried out.

Figure 6 shows isotherm data for zwitterionic HD and DPPC, plus thirteen HD:DPPC mixtures, representing a total of fifteen different stoichiometries (81). This study used HD and DPPC because they have the same number of carbons in the tail region, thus allowing us to focus on the difference between the head groups.

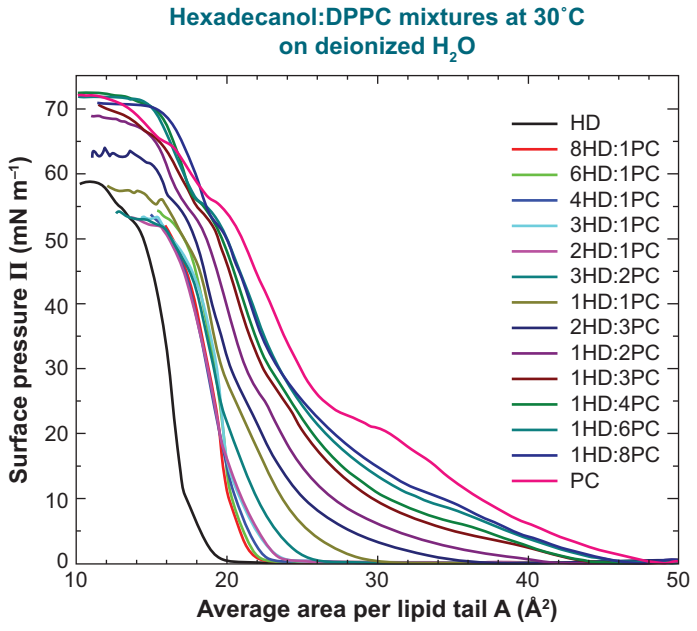

Figure 6

Surface pressure-area isotherms for 15 HD:DPPC mixtures of different stoichiometries at 30°C. The isotherm for HD is shifted to the left by 3 Å^2 for clarity. χ represents χ_{DPPC}, and PC represents DPPC. Figure adapted from Reference 81.

As shown in **Figure 6**, pure HD collapses at ∼60 mN m^{-1}, whereas pure DPPC collapses at ∼70 mN m^{-1} (1, 3). The mixed system distinctly shows a nonmonotonic change in the collapse pressure with varying composition. The addition of DPPC to HD first lowers the collapse pressure at low DPPC content, but a sharp increase to pure DPPC-like values is observed when the mole fraction exceeds ∼0.7. Curiously, a similar threshold value of DPPC content for the increase in collapse pressure is also observed in binary mixtures of DPPC and anionic PA (81). Whereas the cross-sectional area of the head group of DPPC is large compared with that of its tails, the opposite is true for both HD and PA. The question then is why the collapse pressure of the mixed film becomes indistinguishable from that of pure DPPC at and above a DPPC mole fraction, χ_{DPPC} of ∼0.7. Below we show that lateral connectivity between the large DPPC head groups is sufficient to explain the observed phenomenon using a model based on rigidity percolation.

Percolation theory (82, 83) primarily deals with the existence of a connected pathway in lattices whose sites are occupied to different extents. The site-percolation threshold for a 2D lattice is the fraction of lattice sites that needs to be randomly populated until a nearest-neighbor connected cluster spans the entire lattice. The concept of rigidity percolation (84) further extends this idea to vectorial long-range connectivities for estimating the probability of forming not only a spanning cluster but also one that is rigid with respect to applied forces. For a generic 2D lattice, the site-percolation threshold has been estimated to be 0.69755 ± 0.0003 (85).

When a DPPC monolayer is compressed to high pressures, grazing angle X-ray diffraction shows that the lipids have tilted tails (67). Despite the order in the tail regions, there are many degenerate head group configurations associated with a

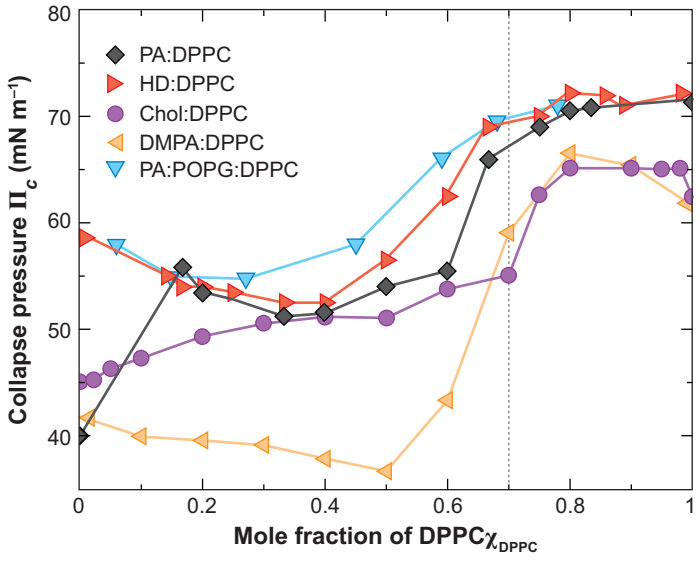

Figure 7

Collapse pressure versus χ_{DPPC}, the mole fraction of DPPC in various mixed monolayers. The data for HD:DPPC and PA:DPPC are from Reference 81, those for Chol:DPPC and DMPA:DPPC are from Reference 86, and the ones for PA:POPG:DPPC are from Reference 87. The dotted line indicates the rigidity site-percolation threshold $\chi_{DPPC} \sim 0.7$.

C domain, leaving even the tail-ordered region with essentially no translational or orientational head group order (10). As the head group is large in DPPC, its size determines the projected area of a DPPC monolayer. The formation of a C DPPC monolayer is thus equivalent to the formation of a random closed-packed 2D lattice of head groups, in other words, a rigid and fully percolated generic 2D lattice (84) of a head group in which the fraction of sites occupied is unity. For a mixed monolayer with either HD or PA, the fraction of lattice sites is reduced, with the empty sites representing much smaller PA or HD head groups. The minimum value of DPPC content for which the monolayer can have the same collapse pressure as DPPC thus becomes the rigidity site-percolation threshold for the generic 2D lattice (81, 85). It is therefore not surprising that the minimum DPPC content for a mixed monolayer to exhibit DPPC-like collapse is found at a χ_{DPPC} of ~0.7.

Because this argument primarily relies on head group arrangements, one can generalize it to any monolayer with similar head-to-tail geometries. Indeed this trend is confirmed by several other studies of collapse involving DPPC:cholesterol (86), DPPC:dimyristoylphosphatidic acid (86), and DPPC:PA:POPG (87). **Figure 7** shows the results of these and the DPPC:PA and DPPC:HD studies. As shown in **Figure 7**, the transition of collapse pressure from the lower to the higher DPPC-like values always occurs approximately at χ_{DPPC} between 0.6 and 0.8. This seemingly universal trend directly supports the simple rigidity percolation treatment (81).

MICROSCOPIC FOLDS AND MACROSCOPIC JERKS

We now return for a moment to the intriguing case of the folding collapse. When the monolayer folds, it gives rise to a sudden, irreversible release of energy that corresponds to a far-from-equilibrium response of the surface film (29, 31, 46, 47, 58,

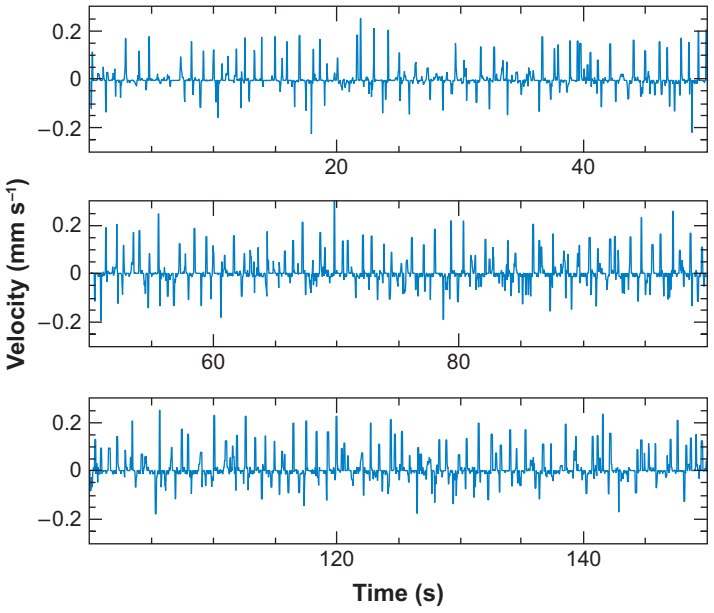

Figure 8

A typical image-analysis signal presented as a seismogram. Shown is the monolayer velocity parallel to the direction of compression as a function of time. The spikes correspond to jerks resulting from out-of-view folding events. Note the large variance of spike heights. The asymmetry between positive and negative translations arises from the asymmetric position of the field of view with respect to the two barriers. Figure adapted from Reference 89.

88). The fold is randomly nucleated at a defect (29, 31, 77, 78) and takes a fraction of a second to form. Although we can see the sequence of folding events in **Figure 2** (47), capturing such images is difficult as it requires the field of view to cover the nucleation site of the collapse, which is impossible to identify a priori. Nonetheless, one can always locate the folds after their formation as each folding event results in a large area of the monolayer translating sharply and uniformly, giving the sense that the monolayer jerks. By repositioning the field of view in the direction of the jerks, one can easily locate the folds.

Combining fluorescence microscopy and digital image analysis, one can follow a large-enough number of jerking events to perform a reliable analysis of the dynamics of folding (89). For a 7:3 DPPC:POPG monolayer at 25°C, collapse sets in at 71 mN m^{-1}, at which the monolayer starts to jerk. **Figure 8** shows the 2D velocity of the monolayer as a function of time, presenting it as a seismogram (89). The jerks, shown as velocity spikes, demonstrate the abruptness of the phenomenon. Each individual jerk is considered an event, and the waiting times between events are the off times, whereas the jerk durations are the on times. When the distribution of off times is plotted, the histogram can be fitted well by an exponential distribution consistent with a Poissonian, uncorrelated sequence of events. Furthermore, the distribution of jerk magnitude is anomalously broad. Whereas the most probable jump spans approximately 2 μm, translations 10 times larger than this still have a nonzero probability of occurring. This is not to be expected given the large variance in the height of the spikes seen in **Figure 8**. The distribution of jerk angles, with zero angle corresponding to motion parallel to the compression direction, further indicates that these folding events are highly anisotropic and that the monolayer can support anisotropic stress like an elastic solid during the off times between events. Analysis

also shows that the jerk angle and the jerk magnitude are anticorrelated in that larger jerks have smaller angles (89). Unlike the magnitude distribution, the distribution of on times is narrow. Although the correlation between the jerk duration and the jerk magnitude shows the expected increasing correspondence (with larger jerks taking longer time), the increase is very weak and follows a logarithmic law. Thus, much larger jerks do not have a correspondingly longer duration. The fact that jerks of largely differing magnitudes have similar durations is consistent with the surprising contrast between the breadth of the magnitude distribution and the narrowness of the on-time distribution observed.

To explain all these peculiar statistics, one needs to interpret each observed jerk as a cascade of folds, in which the cascades have a broad distribution of magnitudes, but each individual fold has a narrowly peaked distribution in its magnitude. A single jerk in effect comprises a cascade of folds of similar size. These statistics are consistent with a description of a cooperative folding cascade occurring in a chain-reaction manner in which the properties of an individual fold are normally distributed, but each fold may topple several next-generation folds, and this may propagate to higher generations of fold in a cascade. The cascades represent unusual nucleation kinetics, in which single-fold growth is macroscopic in one dimension but restricted in another. As a result, a single nucleus cannot fully relax its overstressed environment, hence giving rise to the nucleation of other folds in a chain-reaction manner. This new type of thin-layer failure is not restricted to our specific lipid mixtures or its biphasic structure (31, 88). A fold-and-jerk behavior has been observed in lipid monolayers covering microbubbles (90). Similarly, folding and jerking have been reported for monolayers of nanoparticles at the air-water interface (91).

PERSPECTIVES

This review demonstrates that monolayer collapse can be understood in terms of its materials properties. Fluid monolayers collapse by flowing into the subphase, whereas rigid ones respond by buckling if ductile or cracking if brittle. Future work must concentrate on finding parameters to characterize and quantify the in-plane and out-of-plane rigidity of a given system, which should allow the prediction of the collapse structure in greater detail. The similarity in collapse structures between the many varied phospholipid monolayers and even those of gold nanoparticles begs the question of finding even more general theories to explain this behavior. We believe it is key to extend the continuum arguments already undertaken to larger length scales and focus on the geometric similarities of the systems.

DISCLOSURE STATEMENT

The author is not aware of any biases that might be perceived as affecting the objectivity of this review.

ACKNOWLEDGMENTS

The author is grateful to the many coworkers and collaborators associated with the studies described in this review: V.A. Belyi, H. Diamant, A. Gopal, M.M. Lipp,

T.T. Nguyen, A. von Nahmen, A.J. Waring, D. Wilson, T.A. Witten, and J.A. Zasadzinski. I thank A. Gopal and L. Pocivavsek for their help with the manuscript. I acknowledge support from the University of Chicago MRSEC program of the National Science Foundation (DMR-0213745), the US-Israel Binational Foundation (2002-271), and the March of Dimes (#6-FY07–357).

LITERATURE CITED

1. McConnell HM. 1991. Structures and transitions in lipid monolayers at the air-water interface. *Annu. Rev. Phys. Chem.* 42:171–95
2. Knobler CM, Desai R. 1992. Phase transitions in monolayers. *Annu. Rev. Phys. Chem.* 43:207–36
3. Möhwald H. 1993. Surfactant layers at water surfaces. *Rep. Prog. Phys.* 56:653–85
4. Gelbart WM, Ben-Shaul A, Roux D, eds. 1994. *Micelles, Membranes, Microemulsions, and Monolayers*. New York: Springer-Verlag
5. Safran SA. 1994. *Statistical Thermodynamics of Surfaces, Interfaces, and Membranes*. New York: Addison-Wesley
6. Albrecht O, Gruler H, Sackmann E. 1978. Polymorphism of phospholipid monolayers. *J. Phys.* 39:301–13
7. Andelman D, Brochard F, Knobler C, Rondelez F. 1994. Structures and phase transitions in Langmuir monolayers. See Ref. 4, pp. 559–602
8. Fendler JH, Meldrum FC. 1995. The colloid-chemical approach to nanostructured materials. *Adv. Mater.* 7:607–32
9. Möhwald H. 1995. Phospholipid monolayers. In *Handbook of Biological Physics: Structure and Dynamics of Membranes*, Vol. 1A, ed. R Lipowsky, E Sackmann, pp. 161–211. Amsterdam: Elsevier Sci.
10. Kaganer VM, Möhwald H, Dutta P. 1999. Structure and phase transitions in Langmuir monolayers. *Rev. Mod. Phys.* 71:779–819
11. Flannery D, James SW, Tatam RP, Ashwell GJ. 1997. pH sensor using Langmuir-Blodgett overlays on polished optical fibers. *Opt. Lett.* 22:567–69
12. Flannery D, James SW, Tatam RP, Ashwell GJ. 1999. Fiber-optic chemical sensing with Langmuir-Blodgett overlay waveguides. *Appl. Opt.* 38:7370–74
13. Glasgow BJ, Marshall G, Gasymov OK, Abduragimov AR, Yusifov TN, Knobler CM. 1999. Tear lipocalins: potential lipid scavengers for the corneal surface. *Investig. Ophthalmol. Vis. Sci.* 40:3100–7
14. Greiner JV, Glonek T, Korb DR, Booth R, Leahy CD. 1996. Phospholipids in meibomian gland secretion. *Ophthalmol. Res.* 28:44–49
15. Grace A, Kwok P, Hawke M. 1987. Surfactant in middle ear effusions. *Otolaryngol. Head Neck Surg.* 96:336–40
16. Hills BA. 1984. Analysis of eustachian surfactant and its function as a release agent. *Arch. Otolaryngol.* 110:3–9
17. Veldhuizen R, Nag K, Orgeig S, Possmayer F. 1998. The role of lipids in pulmonary surfactant. *Biochim. Biophys. Acta* 1408:90–108
18. Yu SH, Possmayer F. 2003. Lipid compositional analysis of pulmonary surfactant and monolayer-associated reservoirs. *J. Lipid Res.* 44:621–29

19. Goerke J. 1974. Lung surfactant. *Biochim. Biophys. Acta* 344:241–61
20. Schief WR, Dennis SR, Frey W, Vogel V. 2000. Light scattering microscopy from monolayers and nanoparticles at the air/water interface. *Colloids Surf. A* 171:75–86
21. Lu W, Knobler CM, Bruinsma RF, Twardos M, Dennin M. 2002. Folding Langmuir monolayers. *Phys. Rev. Lett.* 89:146107
22. Lipp MM, Lee KYC, Zasadzinski JA, Waring AJ. 1997. Design and performance of an integrated fluorescence, polarized fluorescence, and Brewster angle microscope Langmuir trough assembly for the study of lung surfactant monolayers. *Rev. Sci. Instrum.* 68:2574–82
23. Angelova A, Vollhardt D, Ionov RJ. 1996. 2D-3D transformations of amphiphilic monolayers influenced by intermolecular interactions: a Brewster angle microscopy study. *Phys. Chem.* 100:10710–20
24. Lu ZH, Nakahara H. 1994. Collapsing processes in stearic-acid monolayer studied by Brewster-angle microscopy. *Chem. Lett.* 11:2005–8
25. Lheveder C, Henon S, Mercier R, Tissot G, Fournet P, Meunier J. 1998. A new Brewster angle microscope. *Rev. Sci. Instrum.* 69:1446–50
26. Schief WR, Hall SB, Vogel V. 2000. Spatially patterned static roughness superimposed on thermal roughness in a condensed phospholipid monolayer. *Phys. Rev. E* 62:6831–37
27. Schief WR, Touryan L, Hall SB, Vogel V. 2000. Nanoscale topographic instabilities of a phospholipid monolayer. *J. Phys. Chem. B* 104:7388–93
28. Schief WR, Antia M, Discher BM, Hall SB, Vogel V. 2003. Liquid-crystalline collapse of pulmonary surfactant monolayers. *Biophys. J.* 84:3792–806
29. Gopal A, Lee KYC. 2001. Morphology and collapse transitions in binary phospholipid monolayers. *J. Phys. Chem. B* 105:10348–54
30. Hatta E, Fischer TM. 2002. Modulation crack growth and crack coalescence upon Langmuir monolayer collapse. *J. Phys. Chem. B* 106:589–92
31. Ybert C, Lu W, Möller G, Knobler CM. 2002. Collapse of a monolayer by three mechanisms. *J. Phys. Chem. B* 106:2004–8
32. Shapiro DL, Notter RH. 1989. *Surface Replacement Therapy*. New York: Liss
33. Gaines GL. 1996. *Insoluble Monolayers at Liquid-Gas Interfaces*. New York: Interscience
34. Bibo AM, Knobler CM, Peterson IR. 1991. A monolayer phase miscibility comparison of long-chain fatty acids and their ethyl esters. *J. Phys. Chem.* 95:5591–99
35. Nikomarov ES. 1990. A slow collapse of a monolayer spread on an aqueous surface. *Langmuir* 6:410–14
36. Vollhardt D. 1993. Nucleation and growth in supersaturated monolayers. *Adv. Colloid Interface Sci.* 47:1–23
37. Tchoreloff P, Gulik A, Denizot B, Proust JE, Puisieux F. 1991. A structural study of interfacial phospholipid and lung surfactant layers by transmission electron microscopy after Blodgett sampling: influence of surface pressure and temperature. *Chem. Phys. Lipids* 59:151–65
38. Gopal A. 2004. *The collapse of phospholipid Langmuir monolayers: implications for biological surfactant*. PhD thesis. Univ. Chicago

39. Nguyen TT, Gopal A, Lee KYC, Witten TA. 2005. Surface charge relaxation and the pearling instability of charged surfactant tubes. *Phys. Rev. E* 72:051930
40. Ries H, Swift H. 1987. Twisted double-layer ribbons and the mechanism for monolayer collapse. *Langmuir* 3:853–55
41. Siegel S, Honig D, Vollhardt D, Mobius D. 1992. Direct observation of 3-dimensional transformation of insoluble monolayers. *J. Phys. Chem.* 96:8157–60
42. Lipp MM, Lee KYC, Zasadzinski JA, Waring AJ. 1996. Phase and morphology changes in lipid monolayers induced by SP-B protein and its amino-terminal peptide. *Science* 273:1196–99
43. Birdi K, Vu D. 1994. Structures of collapsed lipid monolayers investigated as Langmuir-Blodgett films by atomic force microscopy. *Langmuir* 10:623–25
44. Notter RH, Tabak SA, Mavis RD. 1980. Surface properties of binary mixtures of some pulmonary surfactant components. *J. Lipid Res.* 21:10–22
45. Liu H, Lu RZ, Turcotte JG, Notter RH. 1994. Dynamic interfacial properties of surface excess films of phospholipids and phosphonolipid analogs. 1. Effects of pH. *Colloid Interface Sci.* 167:378–90
46. Ding JQ, Takamoto DY, von Nahmen A, Lipp MM, Lee KYC, et al. 2001. Effects of lung surfactant proteins, SP-B and SP-C, and palmitic acid on monolayer stability. *Biophys. J.* 80:2262–72
47. Takamoto DY, Lipp MM, von Nahmen A, Lee KYC, Waring AJ, Zasadzinski JA. 2001. Interaction of lung surfactant proteins with anionic phospholipids. *Biophys. J.* 81:153–69
48. Bangham A, Morley C, Phillips M. 1979. The physical properties of an effective lung surfactant. *Biochem. Biophys. Acta* 573:552–56
49. Goerke J. 1998. Pulmonary surfactant: functions and molecular composition. *Biochim. Biophys. Acta* 1408:79–89
50. Goerke J, Clements JA. 1986. Alveolar surface tension and lung surfactant. In *Handbook of Physiology, Section 3: The Respiratory System*, Vol. III: *Mechanics of Breathing (Part I)*, ed. AP Fishman, pp. 247–61. Bethesda, MD: Am. Physiol. Soc.
51. Clements JA. 1962. Surface phenomena in relation to pulmonary function. *Physiologist* 5:11–28
52. Holm BA, Wang ZD, Egan EA, Notter RH. 1996. Content of dipalmitoyl phosphatidylcholine in lung surfactant: ramifications for surface activity. *Pediatr. Res.* 39:805–11
53. Watkins JC. 1968. The surface properties of pure phospholipids in relation to those of lung extracts. *Biochim. Biophys. Acta* 152:293–306
54. Hildebran JN, Goerke J, Clements JA. 1979. Pulmonary surface film stability and composition. *J. Appl. Physiol.* 47:604–11
55. Hawco MS, Davis PJ, Keough KMW. 1981. Lipid fluidity in lung surfactant: monolayers of saturated and unsaturated lecithins. *J. Appl. Physiol.* 51:509–15
56. Egbert J, Sloot H, Mazure A. 1989. Minimal surface tension, squeeze-out and transition temperatures of binary mixtures of dipalmitoylphosphatidylcholine and unsaturated phospholipids. *Biochim. Biophys. Acta* 1002:109–13

57. Pastrana-Rios B, Flach CR, Brauner JW, Mautone AJ, Mendelsohn R. 1994. A direct test of the "squeeze-out" hypothesis of lung surfactant function: external reflection FTIR at the air-water interface. *Biochemistry* 33:5121–27
58. Lipp MM, Lee KYC, Takamoto DY, Zasadzinski JA, Waring AJ. 1998. Coexistence of buckled and flat monolayers. *Phys. Rev. Lett.* 81:1650–53
59. Bourdieu L, Daillant J, Chatenay D, Braslau A, Colson D. 1994. Buckling of polymerized monomolecular films. *Phys. Rev. Lett.* 72:1502–5
60. Saint-Jalmes A, Graner F, Gallet F, Houchmandzadeh B. 1994. Buckling of a bidimensional solid. *Europhys. Lett.* 28:565–71
61. Hu JG, Granek R. 1996. Buckling of amphiphillic monolayers induced by head-tail asymmetry. *J. Phys. II* 6:999–1022
62. Milner ST, Joanny JF, Pincus P. 1989. Buckling of Langmuir monolayers. *Europhys. Lett.* 9:495–500
63. Tanaka Y, Takei T, Aiba T, Masuda K, Kiuchi A, Fujiwara T. 1986. Development of synthetic lung surfactants. *J. Lipid Res.* 27:475–85
64. von Nahmen A, Schenk M, Sieber M, Amrein M. 1997. The structure of a model pulmonary surfactant as revealed by scanning force microscopy. *Biophys. J.* 72:463–69
65. Schürch S, Green FHY, Bachofen H. 1998. Formation and structure of surface films: captive bubble surfactometry. *Biochim. Biophys. Acta* 1408:180–202
66. Lipp MM. 1997. *A microscopy study of model lung surfactant monolayers*. PhD thesis. Univ. Calif., Santa Barbara
67. Lee KYC, Gopal A, von Nahmen A, Zasadzinski JA, Majewski J, et al. 2002. Influence of palmitic acid and hexadecanol on the phase transition temperature and molecular packing of dipalmitoylphosphatidylcholine monolayers at the air-water interface. *J. Chem. Phys.* 116:774–83
68. Helm CA, Möhwald H, Kjaer K, Als-Nielsen J. 1987. Phospholipid monolayers between fluid and solid states. *Biophys. J.* 52:381–90
69. Brezesinski G, Dietrich A, Struth B, Böhm C, Bouwman WG, et al. 1995. Influence of ether linkages on the structure of double chain phospholipid monolayers. *Chem. Phys. Lipids* 76:145–57
70. Lautz C, Fischer TM, Weygand M, Losche M, Howes PB, Kjaer K. 1998. Determination of alkyl chain tilt angles in Langmuir monolayers: a comparison of Brewster angle autocorrelation spectroscopy and X-ray diffraction. *J. Chem. Phys.* 108:4640–46
71. Brezesinski G, Kaganer VM, Mohwald H, Howes PB. 1998. Structure of octadecanol monolayers: an X-ray diffraction study. *J. Chem. Phys.* 109:2006–10
72. Lipp MM, Lee KYC, Waring AJ, Zasadzinski JA. 1997. Fluorescence, polarized fluorescence, Brewster angle microscopy of palmitic acid and lung surfactant protein B monolayers. *Biophys. J.* 72:2783–804
73. Piknova B, Schief WR, Vogel V, Discher BM, Hall SB. 2001. Discrepancy between phase behavior of lung surfactant phospholipid and the classical model of surfactant function. *Biophys. J.* 81:2172–80
74. Leibler S. 1989. Equilibrium statistical mechanics of fluctuating films and membranes. In *Statistical Mechanics of Membranes and Surfaces*, ed. D Nelson, T Piran, S Weinberg, pp. 45–103. Singapore: World Sci.

75. Wurger A. 2000. Bending elasticity of surfactant films: the role of the hydrophobic tails. *Phys. Rev. Lett.* 85:337–40
76. Guttman GD, Andelman D. 1993. Electrostatic interactions in two-component membranes. *J. Phys. II* 3:1411–25
77. Diamant H, Witten TA, Gopal A, Lee KYC. 2000. Unstable topography of biphasic surfactant monolayers. *Europhys. Lett.* 52:171–77
78. Diamant H, Witten TA, Ege C, Gopal A, Lee KYC. 2001. Topography and instability of monolayers near domain boundaries. *Phys. Rev. E* 63:061602
79. Schief WR, Touryan L, Hall SB, Vogel V. 2000. Nanoscale topographic instabilities of a phospholipid monolayer. *J. Phys. Chem. B* 104:7388–93
80. Schief WR, Hall SB, Vogel V. 2000. Spatially patterned static roughness superimposed on thermal roughness in a condensed phospholipid monolayer. *Phys. Rev. E* 62:6831–37
81. Gopal A, Lee KYC. 2006. Headgroup percolation and collapse of condensed Langmuir monolayers. *J. Phys. Chem. B* 110:22079–87
82. Grimmett G. 1999. *Percolation*. New York: Springer-Verlag. 2nd ed.
83. Stauffer D, Aharony A. 1992. *Introduction to Percolation Theory*. Washington, DC: Taylor & Francis. 2nd ed.
84. Jacobs DJ, Thorpe MF. 1995. Generic rigidity and percolation: the pebble game. *Phys. Rev. Lett.* 75:4051–54
85. Jacobs DJ, Thorpe MF. 1996. Generic rigidity percolation in two dimensions. *Phys. Rev. E* 53:3682–93
86. Albrecht O, Gruler H, Sackmann E. 1981. Pressure-composition phase diagrams of cholesterol-lecithin, cholesterol-phosphatidic acid, and lecithin-phosphatidic acid mixed monolayers: a Langmuir film balance study. *J. Colloid Interface Sci.* 79:319–38
87. Bringezu F, Ding JQ, Brezesinski G, Zasadzinski JA. 2001. Changes in model lung surfactant monolayers induced by palmitic acid. *Langmuir* 17:4641–48
88. Zhang Y, Fischer TM. 2005. Fold-speed control in collapsing mixed phospholipid monolayers. *J. Phys. Chem. B* 109:3442–45
89. Gopal A, Belyi VA, Diamant H, Witten TA, Lee KYC. 2006. Microscopic folds and macroscopic jerks in compressed lipid monolayers. *J. Phys. Chem. B* 21:10220–23
90. Pu G, Borden MA, Longo ML. 2006. Collapse and shedding transitions in binary lipid monolayers coating microbubbles. *Langmuir* 22:2993–99
91. Schultz DG, Lin XM, Li DX, Gebhardt J, Meron M, et al. 2006. Structure, wrinkling, and reversibility of Langmuir monolayers of gold nanoparticles. *J. Phys. Chem. B* 110:24522–29

Annual Review of
Physical Chemistry

Volume 59, 2008

Contents

Indexes

Errata

An online log of corrections to *Annual Review of Physical Chemistry* articles may be found at http://physchem.annualreviews.org/errata.shtml